

Hybrid metapopulation agent-based epidemiological models for efficient insight on the individual scale: a contribution to green computing

Julia Bicker^a, René Schmieding^b, Michael Meyer-Hermann^b,
Martin J. Kühn^{a,c}

^a*Institute of Software Technology, Department of High-Performance Computing, German Aerospace Center, Cologne, Germany*

^b*Department of Systems Immunology and Braunschweig Integrated Centre of Systems Biology (BRICS), Helmholtz Centre for Infection Research, Brunswick, Germany*

^c*Life and Medical Sciences Institute, University of Bonn, Bonn, Germany*

Abstract

Emerging infectious diseases and climate change are two of the major challenges in 21st century. Although over the past decades, highly-resolved mathematical models have contributed in understanding dynamics of infectious diseases and are of great aid when it comes to finding suitable intervention measures, they may need substantial computational effort and produce significant CO_2 emissions. Two popular modeling approaches for mitigating infectious disease dynamics are agent-based and differential equation-based models. Agent-based models (ABMs) offer an arbitrary level of detail and are thus able to capture heterogeneous human contact behavior and mobility patterns. However, insights on individual-level dynamics come with high computational effort that scales with the number of agents. On the other hand, (differential) equation-based models (EBMs) are computationally efficient even for large populations due to their complexity being independent of the population size. Yet, equation-based models are restricted in their granularity as they assume a (to some extent) homogeneous and well-mixed population. To manage the trade-off between computational complexity and level of detail, we propose spatial- and temporal-hybrid models that use agent-based models only in an area or time frame of interest. To account for relevant influences to disease dynamics, e.g., from outside, due to commuting activities, we use equation-based models, only adding moderate computational costs. Our hybridization approach demonstrates significant reduction in computa-

tional effort by up to 98% – without losing the required depth in information in the focus frame. The hybrid models used in our numerical simulations are based on two recently proposed models, however, any suitable combination of ABM-EBM could be used, too. Concluding, hybrid epidemiological models can provide insights on the individual scale where necessary, using aggregated models where possible, thereby making an important contribution to green computing.

Keywords:

1. Introduction

Two of the major 21st century’s challenges are accelerating climate change [1] and emerging infectious diseases with an expected increase in frequency of epidemics and pandemics [2]. As these challenges are driven by the same underlying causes, sets of proposed counteractions might go hand-in-hand [2, 3]. In order to assess counteractions and support decision-makers, mathematical models are viable tools that have been used extensively in both domains. Models can help to understand the situation at hand and to analyze potential future developments, which often cannot be conducted in classical experiments. The recent COVID-19 pandemic has demonstrated the benefit of mathematical models to analyze ongoing infectious disease dynamics and to evaluate potential scenarios, see, e.g., [4, 5, 6]. Extensive testing strategies maintaining mobility as a social good, have, for instance, been studied in [7]. The set of mathematical models to epidemiological emergencies is diverse and ranges from classical statistical models such as generalized regression models, through equation-based [4, 8], metapopulation [9, 10], and agent-based [11, 5, 12, 13] models to machine and deep learning models [14, 15]. Equation- or metapopulation-based models using sets of ordinary [4, 10] or integro-differential-equation-based models [8] are well established methods that have been used by hundreds of work groups worldwide to analyze infectious disease dynamics. Their advantages are the ease of analysis, their well-understood character and the low computational requirements which do not depend on the number of persons in the population but on the number of different subpopulations. However, their insight on the individual level dynamics or on (singular) stochastic effects is limited and they also fail in the beginning of an outbreak when the number of infected is small. Agent- or individual-based models, on the other hand, allow the stochastic

simulation of individual behavior and reaction to diseases, in a social and immunological dimension, see, e.g., [5, 16]. Though, this comes at the cost of superlinear complexity. While the energy consumption corresponding to computational cost can be reduced through, e.g., optimizations on the cache level [17] or the optimal use of heterogeneous hardware structures such as SIMD registers [18], we here propose a complementary approach to directly avoid less impactful computations through the development of well-designed hybridization concepts.

The authors of [12] demonstrated that the inclusion of disease import, i.e., the infections caused by travelers and commuters, is an important factor to explain disease dynamics. Via the metapopulation approach in [7], it was shown how large the effects of disease import can become if testing is not done properly. Using simple statistics for disease import can be a suitable first step in improving model precision in a considered focus region. However, if disease import is subject to change through interventions, disease dynamics in coupled regions are advised to also be modeled dynamically.

In this work, we will present a generic framework for spatial-and temporal-hybrid epidemiological modeling, combining any pair of suitable fine-granular agent-based and coarse-granular equation- or metapopulation based models. We will then suggest a particular combination of two suitable models suggested recently in [19]. We will present results on a more theoretical quadwell geometry and a more realistic case of the city of Munich with its surrounding counties. In this context, we will simulate a COVID-19-like disease with parameters motivated by [10]. However, as the scope of the current paper is the disease-agnostic introduction of novel hybrid models, no further parameter refinement for COVID-19 has been performed. Let us note that any other disease model can be put in our framework. We will show that our hybrid modeling approach can account for individual developing disease dynamics, otherwise modeled with pure agent-based models, while drastically reducing computational effort. We will provide discussions, limitations, and directions for future research before we eventually draw a conclusion.

2. Materials and methods

In this section, we first introduce generic models. Second, we describe the framework idea of temporal and hybrid modeling which in third place will be realized with a combination of two suitable models.

2.1. Introduction to model types

Models for epidemic, pandemic, or endemic scenarios can be realized in many ways and widely used model types are based on equations, metapopulation, or agent-based approaches. The development of a model or a model selection is always based on the (research) question at hand and all particular models have their corresponding advantages and disadvantages. In the following section, we do not want to focus on a particular model but generically describe different model types. Note furthermore that in this paper, the term equation-based models will be limited to ordinary differential equations (ODEs) although other types of equation-based models are possible.

2.1.1. Equation- and metapopulation-based models

Simple ODE-based models. In the following, we restrict ourselves to equations given by ordinary differential equations (ODEs). In corresponding models, we subdivide the population in different *infection states* or *compartments* and denote the set of infection states as $\mathcal{Z} := \{z_1, \dots, z_{n_I}\}$ with n_I the number of infection states. Let $N_i(t) \in \mathbb{R}_{\geq 0}$ be the number of individuals in infection state $i \in \mathcal{Z}$ and $N(t) = (N_i(t))_{i \in \mathcal{Z}} \in \mathbb{R}_{\geq 0}^{n_I}$ the system state at time t . For each infection state transition or adoption $i \rightarrow j$, i.e., from compartment i to compartment j , we define adoption rate functions $\hat{f}_{i,j} : \mathbb{R}_{\geq 0}^{n_I} \rightarrow \mathbb{R}_{\geq 0}$, $i, j \in \mathcal{Z}$. These are just zero if no adoption from i to j is possible, otherwise, they define the (out)flow from i to j . The adoption dynamics are then given by ordinary differential equations of the form

$$\frac{d}{dt} N_i(t) = \sum_{\substack{j \in \mathcal{Z} \\ i \neq j}} (\hat{f}_{j,i}(N(t)) - \hat{f}_{i,j}(N(t))). \quad (1)$$

We now provide a brief summary on further extensions of the initial model that might be of interest when combined with a particular agent-based model in our hybridization approach.

Sociodemographic stratification. The inherent assumption in the previously introduced formulation is homogeneous mixing of the population. To account for sociodemographic influences, e.g., age-dependent transmission or sex/gender- and income-dependent severity outcomes, we can further subdivide the compartments. Then, e.g., $z_{i,r,s}$, $i = 1, \dots, n_I$, represents infection state z_i for a pair $(r, s) \in \{1, \dots, n_A\} \times \{1, \dots, n_E\}$ in the sociodemographic dimensions age, with n_A groups, and income, with n_E groups. With this

extension, all adoption rates additionally depend on the sociodemographic groups. For an ODE-based model with different age groups, see, e.g., [10].

Contact location stratification. In order to stratify for different contact and transmission settings, we can use location-resolved contact data [20] to subdivide the total number of contacts by contacts in, e.g., school, workplaces, or home locations. For a model with different contact locations, see, e.g., [10].

Circulating pathogens, variants stratification, and immunization history. In case of multiple circulating pathogens or variants of a pathogen like SARS-CoV-2 variants, coexistence and interactions of infections might be considered as well. In this case, one out of many approaches is to use one set of infection states $\mathcal{Z}_l := \{z_1, \dots, z_{n_{I_l}}\}$ for any pathogen or variant $l \in \{1, \dots, n_V\}$. For an example with eight modeled variants in Ethiopia, see [21]. Furthermore, subpopulations with different immunization histories and protection levels can be used [6, 22].

Example. To visualize our generic introduction, we provide an example of the most simple ODE-SIR model without any further stratification. There, we have $\mathcal{Z} = \{S, I, R\}$. The adoption rate functions are, first, $\widehat{f}_{S,I}(t) = \phi \rho N_I(t) \frac{N_S(t)}{n_a}$, where ρ is the average transmission probability per contact, ϕ the average number of contacts in unit time and n_a the total population size. Secondly, we have $\widehat{f}_{I,R}(t) = \frac{N_I(t)}{T_I}$ where T_I is the average time a person stays infected. All other adoption rate functions are zero.

Metapopulation models. Metapopulations can be used to leverage simple, spatially-agnostic ODE-based models to spatially-resolved models. For that, we extend the previous definitions by defining the system state N by $N(t) = \left(N_i^{(k)}(t) \right)_{i \in \mathcal{Z}, 1 \leq k \leq n_R} \in \mathbb{R}^{n_I \times n_R}$ with $N_i^{(k)}(t)$ the number of individuals in infection state i and regional entity k . In the following, we simply denote regional entities of any size as regions. The adoption rate functions $f_{i,j}^{(k)}$ are then also dependent on region k and can be defined differently for different approaches.

Implicit exchange between metapopulations. One way of realizing spatial resolution is modeling regional influences implicitly through inclusion of external populations in the adoption rate functions $\widehat{f}_{i,j}^{(k)}$ through $\widehat{f}_{i,j}^{(k)} : \mathbb{R}_{\geq 0}^{n_I \times n_R} \rightarrow \mathbb{R}_{\geq 0}$. That means the local population $\left(N_i^{(k)}(t) \right)_{i \in \mathcal{Z}}$ is only implicitly influenced by $N_i^{(l)}$ through $\widehat{f}_{i,j}^{(k)}$, $l \neq k$. An important property of this approach is that

the global infectious disease dynamics can be modeled within one larger ODE system. A corresponding model can be found in, e.g, [9].

Explicit exchange between metapopulations. A contrasting approach to realize metapopulation models is to explicitly exchange local populations. This can be done by combining initially decoupled equations giving disease dynamics in the different regions with a particular mobility model that explicitly changes the populations $N_i^{(k)}$ at discrete time points $t_s \in [0, \infty)$. Introducing spatial exchange functions $g_i^{(k,l)} : [0, \infty) \rightarrow \mathbb{R}$ for any pair of regions (k, l) , $k \neq l$ and infection state $i \in \mathcal{Z}$, we define

$$N_i^{(k)}(t_s) = N_i^{(k)}(t_s) + \sum_{l \neq k} g_i^{(k,l)}(t_s). \quad (2)$$

The updated values for $N_i^{(k)}$ are then used to simulate from t_s until the next discrete exchange point. In these cases, we can define adoption rate functions on the space of local populations as $\widehat{f}_{i,j}^{(k)} : \mathbb{R}_{\geq 0}^{n_I} \rightarrow \mathbb{R}_{\geq 0}$. Note that in these approaches, we explicitly have noncontinuous subpopulation trajectories and numerical integrators have to be stopped and restarted at exchange points. However, when only a limited number of discrete exchange points are chosen, the increased number of restarts is not to be considered critical. Corresponding models can be found in [10, 19]. While the authors of [10] use a deterministic approach to ensure that return travel is made at predefined time points with a close approximation of initial commuters, the authors of [19] use stochastic jump processes for spatial exchange without enforcing corresponding returns.

Remark 1. *Note that the previous classification and metapopulation examples are guided by the referenced papers and might only offer an incomplete view as also other approaches could be possible. For instance, one could also think of realizing explicit mobility exchange within one large ODE system.*

2.1.2. Agent-based models

The nature of agent-based modeling is to capture more intuitively and to model in a direct manner individual (human) properties and interactions. Corresponding models have already been explored before the availability of modern computers; see, e.g., [23]. The authors of [24] have set up a so far nonexisting taxonomy for agent-based models (ABMs) in infectious diseases and considered if particular ABMs included modules or submodels for society, transportation, and environment.

Remark 2. *In the following, we provide our understanding of an ABM. An agent-based model (ABM) consists of a finite number of agents $\alpha_1, \dots, \alpha_{n_a}$ and an environment in which and to which an agent reacts. Furthermore,*

- *an agent is characterized by a finite number of features that determine an agent's state,*
- *an agent interacts with other agents and their joint environment according to interaction rules,*
- *the state of an agent or the environment changes through interactions or with time.*

The previously introduced stratifications for equation-based models can be realized in ABMs directly through features of the agents. These can comprise the age, sex/gender, income, infection state, or immunization history. In particular, infection states or immunization history can directly be enriched with information on the particular pathogen or virus and the virus variant.

Also in contrast to equation-based modeling, many states from features naturally live or can live on a continuous (e.g., a location or a position, timings of past infections or vaccinations) or fine-granular discrete (e.g., age in years) scale.

2.2. A framework of hybrid modeling

The essential motivation to use equation-based models combined with agent-based models for disease dynamics is to reduce the computational effort of a model on individual level which scales superlinear with the number of considered agents or individuals.

We introduce two different types of hybrid epidemiological models: spatial-hybrid and temporal-hybrid models. These approaches do not exclude each other so that also spatio-temporal-hybrid models can be realized. Both hybridization approaches are shown in Fig. 1.

A requirement to the two models used is that we can define a mapping between them. In its simplest form, the coarse-granular model may be obtained by projection from the fine model. In a more elaborated setting, we need to map fine-granular, continuous features like viral load to a discrete, coarse-granular definition. Naturally, going from fine-to-coarse is easier as information gets reduced. Going from coarse-to-fine either needs sampling

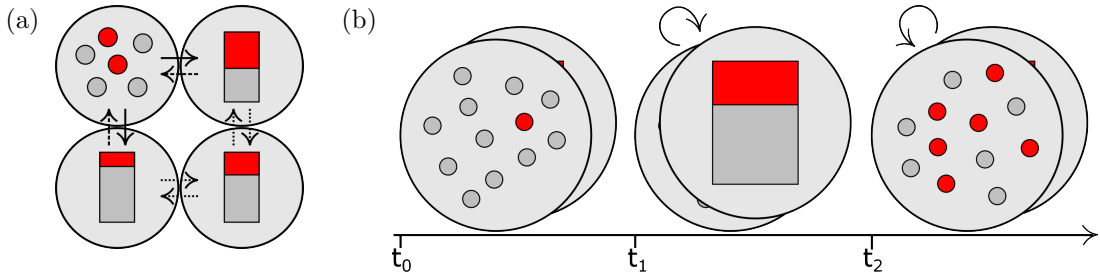


Figure 1: **Design sketch of a spatial-hybrid model (a) and a temporal-hybrid model (b).** Large gray disks represents (sub)regions, with possible population exchanges indicated by arrows. The population is represented by small disks for agents and bar charts for ODE compartments. Red indicates infected agents or population shares, gray indicates noninfected agents or population shares. The exchange in (a) only moves small parts of a local population to another region, the exchange in (b) moves the entire population to the other model.

or the replication of retained information to realize a realistic model over the whole simulation horizon (spatial or temporal). Furthermore, both model types should match in the sense that for reasonable parameters, their results are on average similar enough (with respect to some tolerance).

Remark 3. *Note that the term hybrid is already used for metapopulation models that are connected by a a graph or network, as, e.g., in [25, 10]. Similar hybrid approaches are also presented in [26, 27]. In this paper, we present another understanding of hybrid models in the spatial sense by allowing different model types in different regions.*

2.2.1. Spatial hybridization

The idea of a *spatial-hybrid model* originates from research questions on fine-granular infection spread, like household or workplace transmission in a particular region. To consider only this (focus) region would neglect the influence of connected regions on infection dynamics through, e.g., commuting activities. However, the use of fine-granular models for all connected regions might be prohibitively expensive or individual-level data is either exclusively available in the focus region, or substantially costly to collect for outside regions.

The focus region is then modeled by a fine-granular model and we use coarse-granular models in any connected region. With this approach we get results with the desired resolution in the focus region while considering the dynamic, time-dependent influence of the connected regions in a runtime

efficient manner. In the following, we will denote this approach as *spatial hybridization* and will refer to hybrid models with higher granularity in a focus region as *spatial-hybrid models*.

For the spatial hybridization, we require a disjoint partition of the modeled domain into at least two subregions. The exchange of populations between the different regions can be realized with different mobility models, however, sending agents to a coarser model does cause loss of information (e.g. sending an agent to a simple ODE-based model will only retain its infection state and lose all spatial information). To the best of our knowledge, there is only little theory on this exchange problem and the exchange is highly dependent on the concrete models used. Some discussions and suggested models can be found in [28, 25, 29].

In the introduction of this section, we formulated that both model types should match in some sense regarding average outcomes. On one hand, ODE-based models are not able to let a virus go completely extinct. On the other hand, ABMs can simulate this extinction. This does not mean that a spatial-hybrid of ODE-ABM cannot be used if infection numbers are small in one region, only that the results may differ from the results of a fully fine-resolved (stochastic) model and hence that this needs to be considered when evaluating simulation results. For further discussion on this effect, see e.g. [30, 31]. More suitable combinations could use stochastic differential equation-based models or a mixed spatial-temporal-hybrid (in combination with the next section).

Two ways to obtain compatible models are to fit the two models against each other, or to derive the coarse model (parameters) from the fine one. However, in both cases it is important to understand the model behavior very well to be aware of inter-dependencies. For instance, location and infection state changes may depend on each other and cannot always be fitted separately. An interesting discussion can be found in [32].

2.2.2. Temporal hybridization

The idea of *temporal-hybrid models* is based on the assumption that the lower the case numbers, the higher is the impact of stochastic events to the (simulation) outcome. On the other hand, if case numbers are high, individual behavior and stochastic events become less influential. This means that single simulation results of stochastic models come closer to averaged outcomes.

The temporal hybridization is based on the same requirements as the

spatial-hybrid model, except that we only use one model for the whole domain and switch between coarse- and fine-granular model during the course of the simulation. Then, instead of exchanging agents or populations on spatial transitions, we exchange the entire model at certain time points. These time points depend on the current system state and are thus selected dynamically. In the consequence, we need fine granular data for the whole domain.

In Section 2.4.2, we use an ABM to model disease spread when the number of infected individuals is below a predefined threshold and switch to a coarser, hence ODE-based or metapopulation model, as soon as the number of infected individuals exceeds the threshold. In literature this kind of hybrid model is also referred to as stage-based hybrid model, see e.g. [25] and [28]. We call this approach *temporal hybridization* and the corresponding model a *temporal-hybrid model*.

In case of the virus-extinction example from above, we could change from an ODE-based or metapopulation model to an ABM whenever the number of virus carriers drops below a threshold that would realistically allow an extinction to occur and switch back whenever the virus will, with some certainty or probability, spread to a larger population. Note that this approach needs careful evaluation of the switching condition. Like for the spatial-hybrid model the exchange of information between models is crucial and dependent on the concrete models used. A benefit of a temporal-hybrid model is that it can effectively save computational cost in periods of diffusive spread while maintaining the required level of detail in highly stochastic periods.

2.3. Explicit models

In this section, we will present two models that were introduced by [33] for which we define infection states and possible courses of the disease used in both model types, fine- and coarse-granular. We start with an ABM, whose change over time is described by a master equation motivated by chemical reaction systems, cf., e.g., [34]. While this does impose some restriction on what the agents' (inter)actions may be, it allows us to derive a piecewise deterministic metapopulation model (PDMM) that shares parameters and behavior with the ABM. As the PDMM can be obtained by a model reduction of the presented ABM, the models fulfill the requirements presented in Section 2.2. In this section, we focus on the theoretical formulation. All models are implemented on a fork of the MEmilio software [35] for modular epidemics simulations.

2.3.1. A diffusion- and drift-based agent-based model

The main features of the used ABM are the infection dynamics and agents' movements. Agents are represented as a tuple $(x, z) \in \Omega \times \mathcal{Z}$, where $\Omega \subset \mathbb{R}^2$, the environment, is a compact domain and $\mathcal{Z} = (z_1, z_2, \dots, z_{n_I})$ a set of infection states. Considering n_a agents, the system state is defined as a vector $Y := (X, Z) \in \mathbb{Y} := \Omega^{n_a} \times \mathcal{Z}^{n_a}$, where an agent α (with its two features, position and infection state) is represented by the α -th component of the system state $Y_\alpha = (x_\alpha, z_\alpha) = (X, Z)_\alpha$. The evolution of the system state over time is modeled as a continuous-time Markov process $(Y(t), t \geq 0)$. The evolution of the process is determined by a so called master equation, that describes the relevant probability measure by the change of its probability density

$$\partial_t p(X, Z; t) = Gp(X, Z; t) + Lp(X, Z; t). \quad (3)$$

The operator G defines the infection state adoptions and only acts on Z , while L defines location changes, only acting on X .

We now want to define both operators, starting with G . To that end, let $i \rightarrow j$ be an infection state adoption, where $i \in \mathcal{Z}$ is the current infection state, and $j \in \mathcal{Z} \setminus \{i\}$ the infection state to adopt. For any particular agent, we assume that the likelihood of this adoption to happen in a given amount of time is determined by some rate $f_{i,j}^{(\alpha)}(Y(t))$ depending on the system state at the current time t . We call this rate (*infection state*) *adoption rate*. A suitable method to realize this rate-dependent infection dynamic is using independent inhomogeneous Poisson processes $\mathcal{P}_{i,j}(t) := \mathcal{P}_{f_{i,j}^{(\alpha)}(Y(t))}$ for infection state adoption $i \rightarrow j$ and agent α . As a natural extension of $f_{i,j}^{(\alpha)}$, for $j = i$, we define $f_{i,i}^{(\alpha)} \equiv 0$. These rates should be interpreted as rates to change the current state.

For a given infection state adoption, various compartments can influence the adoption rate. The influence of an adoption $i \rightarrow j$ is defined as an index set $\Psi_{i,j} \subset \mathcal{Z} \setminus \{i\}$. We use these influences to differentiate between two types of adoptions:

1. First-order adoption: An adoption event that does not require interactions with other agents, i.e., spontaneous infection state change, like recovery or death from the disease. Its adoption rate only depends on the compartment the agent is currently in, thus $\Psi_{i,j} = \emptyset$.
2. Second-order adoption: An adoption based on pairwise interactions, i.e., infection via a contact with an infectious agent. The rate depends

on the compartment of origin of an agent as well as all influences in $\Psi_{i,j} \neq \emptyset$.

Therefore, if there are no influences, the adoption event is of first-order, and of second-order if there are any.

The adoption rates are given by adoption rate functions $f_{i,j} : \mathbb{Y} \rightarrow [0, \infty)^{n_a}$, which in general depend on the whole system state. For each agent α , the α -th component of $f_{i,j}$ is given by the function $f_{i,j}^{(\alpha)} : \mathbb{Y} \rightarrow [0, \infty)$, which depending on the order of the adoption $i \rightarrow j$ is defined as

$$f_{i,j}^{(\alpha)}(X, Z) = \delta_i(z_\alpha) \gamma_{i,j}(x_\alpha) \quad (4)$$

for first-order adoption events, or

$$f_{i,j}^{(\alpha)}(X, Z) = \delta_i(z_\alpha) \sum_{\tau \in \Psi_{i,j}} \sum_{\beta=1}^{n_a} \delta_\tau(z_\beta) \gamma_{i,j,\tau}(x_\alpha, x_\beta) \quad (5)$$

for second-order adoptions. Here $\delta_i(z_\alpha)$ is the Kronecker-delta, being 1 when agent α has infection state i and 0 otherwise. The functions $\gamma_{i,j} : \Omega \rightarrow [0, \infty)$ and $\gamma_{i,j,\tau} : \Omega^2 \rightarrow [0, \infty)$ give the magnitude of the adoption rate, only depending on an agent's position. For example, we can choose

$$\gamma_{i,j}(x) = c_{i,j} \text{ and } \gamma_{i,j,\tau}(x, y) = c_{i,j,\tau} \mathbb{1}_{\|x-y\|_{\Omega} \leq r} , \quad (6)$$

with a cutoff for second-order adoptions beyond the interaction radius $r > 0$. The radius determines how close two agents have to be for being considered contacts, and we use rate constants $c_{i,j} \geq 0$, $c_{i,j,\tau} \geq 0$. We always set $c_{i,i} = c_{i,i,\tau} = 0$ as adoptions from one state to itself are not possible. Note that rate constants $c_{i,j}$ and $c_{i,j,\tau}$ could also be time-varying $c_{i,j}(t)$ and $c_{i,j,\tau}(t)$. Since the adoption rates are not dependent on a particular agent (i.e., a vector component Y_α), we can measure adoptions independently. Hence, the operator G is defined by summation over all components as follows:

$$\begin{aligned} Gp(X, Z; t) := & - \sum_{i,j=1}^{n_I} \sum_{\alpha=1}^{n_\alpha} f_{i,j}^{(\alpha)}(X, Z) p(X, Z; t) \\ & + \sum_{i,j=1}^{n_I} \sum_{\alpha=1}^{n_\alpha} f_{i,j}^{(\alpha)}(X, Z + je_\alpha - ie_\alpha) p(X, Z + je_\alpha - ie_\alpha; t), \end{aligned} \quad (7)$$

where e_α is the α -th standard basis vector.

Similarly, for the location changes, we have the component-wise changes

$$L_i^{(\alpha)}[p(x, z, t)] := p(y_i(t), z, t), \quad (8)$$

where y_i is the trajectory of an agent α with infection state $i \in \mathcal{Z}$ and initial position $x \in \Omega$. We will use independent diffusion processes to determine y_i . In general $L_i^{(\alpha)}$ can almost be chosen arbitrarily, but, for the derivation of the corresponding coarse-granular model presented in the next section, $L_i^{(\alpha)}$ is chosen such that (11) can be solved analytically. Further, define $L^{(\alpha)}$ for X such that it acts as $L_i^{(\alpha)}$, but only on x_α , the α -th component of X . Lastly, we define the movement operator L as

$$Lp(X, Z, t) := \sum_{\alpha=1}^{n_a} L_\alpha p(X, Z, t). \quad (9)$$

As mentioned above, agents' movement trajectories y (omitting the dependency i) will be determined by independent diffusion processes. They are given by stochastic differential equations of the form

$$\frac{dx(t)}{dt} = b(t, x(t)) + \sigma(t, x(t))\xi(t). \quad (10)$$

Here, $b : [0, T] \times \mathbb{R}^2 \rightarrow \mathbb{R}^2$ is a potential on the domain, also called drift coefficient, and $\sigma : [0, T] \times \mathbb{R}^2 \rightarrow \mathbb{R}^{2 \times m}$ is called diffusion coefficient or noise. The potential can be given by a function $F : \Omega \rightarrow \mathbb{R}$ in which case $b := -\nabla F$. As F is assumed to be deterministic, all random behaviour is solely caused by the noise. The magnitude of the noise determines the influence of the white noise process $\xi : [0, T] \rightarrow \mathbb{R}^m$ on the diffusion. Formally, it is defined as $\xi = \frac{dW}{dt}$, the derivative of the Brownian motion in \mathbb{R}^m . The parameter m can be used to stratify agents' movement, for example with respect to infection state or region.

In practice, we use an agent's current position as initial value for (10), and only integrate a small time step to get its new position.

2.3.2. The corresponding piecewise deterministic metapopulation model

The corresponding piecewise deterministic metapopulation model (PDMM) simplifies the ABM by using two approximations. In the following, we will shortly describe these approximations. The full derivation of the PDMM from the ABM introduced above can be found in [19].

First, computational effort is reduced by discretizing the domain. The domain is split into subregions $\Omega_1, \dots, \Omega_{n_R}$ with $\Omega = \bigcup_{k=1}^{n_R} \Omega_k$ and agents are aggregated to subpopulations in the subregions. Hence, an agent's position is now defined only by its subregion index $k \in \{1, \dots, n_R\}$ instead of an exact position $x \in \Omega$. Consequently, all agents in one subregion have the same position. Like described in Section 2.1.1, the system state is defined as the matrix $N = (N_i^{(k)})_{i \in \mathcal{Z}, k=1, \dots, n_R} \in \mathbb{R}_{\geq 0}^{n_I \times n_R}$, with $N_i^{(k)}$ the number of agents in region Ω_k and compartment i . Let $e_i^{(k)}$ be the matrix where the entry for (i, k) is 1 and all others are 0. The movement between subpopulations is modeled by Poisson processes $\mathcal{L}_i^{(k,l)}$ with rates $\lambda_i^{(k,l)}$ for spatial transitions from subregion k to l , $k, l \in \{1, \dots, n_R\}$. These rates depend on the transitioning agent's infection state i and are of the form $N \rightarrow N + e_i^{(l)} - e_i^{(k)}$. Formally, the spatial transition rates are given by the location change operator L through

$$\lambda_i^{(k,l)} := \frac{\int_{\Omega} \delta_{\Omega_l}(x) L_i[\delta_{\Omega_k}(x)] dx}{\int_{\Omega} \delta_{\Omega_k}(x) dx}, \quad (11)$$

but in practice they may be easier to sample than to calculate analytically. The space of all possible system states is given by

$$\mathbb{M}_{n_a} = \left\{ N \left| \sum_{i=1}^{n_I} \sum_{k=1}^{n_R} N_i^{(k)} = n_a \right. \right\}, \quad (12)$$

where n_a is again the total number of agents in the model.

Secondly, model and computational cost is reduced by approximating the infection state adoption processes by a deterministic system of equations. The underlying assumption is that the populations are large such that infection state adoptions are relatively rapid and spatial transitions are comparatively rare. Using region-dependent adoption rate functions $\widehat{f}_{i,j}^{(k)} : \mathbb{R}_{\geq 0}^{n_I} \rightarrow \mathbb{R}_{\geq 0}$, the adoption dynamics are given by ordinary differential equations of the form

$$\frac{d}{dt} N_i^{(k)}(t) = \sum_{\substack{j \in \mathcal{Z} \\ i \neq j}} (\widehat{f}_{j,i}^{(k)}(N^{(k)}(t)) - \widehat{f}_{i,j}^{(k)}(N^{(k)}(t))), \quad (13)$$

without accounting for spatial transitions; cf. (1). The evolution of the system state $N(t)$ over time is described by a continuous-time Markov jump

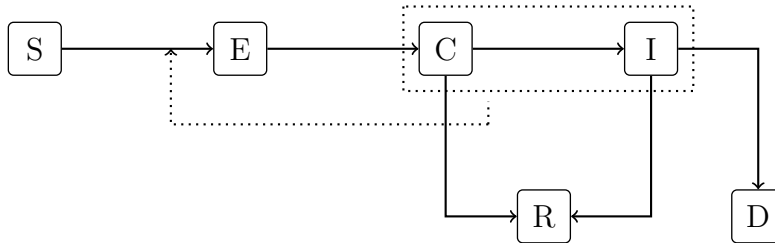


Figure 2: **Flow chart of the adoption model.** The dotted lines shows the influences for the second-order adoption.

process. Writing $(N(t))_{t \geq 0}$ as a path, we obtain

$$\begin{aligned}
 N(t) = N(0) + \sum_{\substack{k,l=1 \\ k \neq l}}^{n_R} \sum_{i=1}^{n_I} \mathcal{L}_i^{(k,l)} \left(\int_0^t \lambda_i^{(k,l)} N_i^{(k)}(s) ds \right) (e_i^{(l)} - e_i^{(k)}) \\
 + \sum_{k=1}^{n_R} \sum_{i,j=1}^{n_I} \int_0^t \widehat{f}_{i,j}^{(k)}(N(s)) ds (e_j^{(k)} - e_i^{(k)}) .
 \end{aligned} \tag{14}$$

For the full derivation from the ABM through a stochastic metapopulation model to the PDMM using convergence results for Markov processes, see again [19].

2.3.3. Transmission and course of the disease

As course of the disease model, we use a Susceptible-Exposed-Carrier-Infected-Recovered-Dead model, thus $\mathcal{Z} = (S, E, C, I, R, D)$. Individuals in the *Carrier* compartment may be either pre- or asymptomatic, hence they do not show symptoms while the *Infected* compartment encompasses all individuals showing symptoms ranging from mild to severe. Both compartments are infectious to *Susceptibles*. There is only one second-order adoption (see Fig. 2) which is $S \rightarrow E$ with influences $\Psi_{SE} = \{C, I\}$. As there is no outflow from the *R* compartment, this model does not consider the possibility of reinfection.

Given the courses of the disease and transmission possibilities defined here, the local equations giving the adoption dynamics in the different PDMM

regions of Section 2.3.2 write

$$\begin{aligned}
\frac{d}{dt}N_S^{(k)} &= -\frac{\rho^{(k)}\left(\xi_C^{(k)}N_C^{(k)} + \xi_I^{(k)}N_I^{(k)}\right)}{n_a^k}N_S^{(k)}, \\
\frac{d}{dt}N_E^{(k)} &= \frac{\rho^{(k)}\left(\xi_C^{(k)}N_C^{(k)} + \xi_I^{(k)}N_I^{(k)}\right)}{n_a^k}N_S^{(k)} - \gamma_{E,C}^{(k)}N_E^{(k)}, \\
\frac{d}{dt}N_C^{(k)} &= \gamma_{E,C}^{(k)}N_E^{(k)} - (\gamma_{C,R}^{(k)} + \gamma_{C,I}^{(k)})N_C^{(k)}, \\
\frac{d}{dt}N_I^{(k)} &= \gamma_{C,I}^{(k)}N_C^{(k)} - (\gamma_{I,R}^{(k)} + \gamma_{I,D}^{(k)})N_I^{(k)}, \\
\frac{d}{dt}N_R^{(k)} &= \gamma_{C,R}^{(k)}N_C^{(k)} + \gamma_{I,R}^{(k)}N_I^{(k)}, \\
\frac{d}{dt}N_D^{(k)} &= \gamma_{I,D}^{(k)}N_I^{(k)}.
\end{aligned} \tag{15}$$

2.4. Hybridization

We apply the two hybridization approaches described in Section 2.2 to the introduced models of Section 2.3.1 and Section 2.3.2. As the motivation emerges from combining a coarser model (PDMM) with a detailed model (ABM) to manage the high computational costs of individual-scale models, we give a short overview of the computational costs with respect to the number of agents n_a . For both models, we need to consider computational costs for spatial transitions or movements and infection state adoption dynamics. The movement of agents in the ABM is given by a diffusion process that has to be evaluated for every agent. Assuming a constant time for the evaluation, the cost to calculate movement dynamics in the ABM lies in $\mathcal{O}(n_a)$. Furthermore, the infection state adoption rates have to be evaluated in every iteration. As first order adoption rates are computed per agent, the complexity as well is in $\mathcal{O}(n_a)$. For second-order adoptions, pairwise comparison of agents is necessary, hence, we obtain a superlinear complexity and in the worst case one iteration has computational cost in $\mathcal{O}(n_a^2)$. For the PDMM the cost for infection state adoption dynamics in one iteration is given by integrating the system of differential equations, it is thus independent of n_a . Technically, the cost for integration scales with the number of equations meaning the number of regions and compartments, but their size is negligibly small compared to n_a . Therefore, the relevant complexity and runtime factor in the PDMM is given by the spatial transition events. The frequency of the

spatial transitions depends on the magnitude of the rates. As the transition rates are multiplied with the corresponding subpopulation, see (14), the complexity of the spatial dynamics lies in $\mathcal{O}(n_a)$. A summary of the model characteristics is given in Table 1.

	ABM	PDMM
<i>Complexity</i>	superlinear, up to $\mathcal{O}(n_a^2)$	$\mathcal{O}(n_a)^*$
<i>Spatial domain</i>	continuous	discrete
<i>Adoption dynamics</i>	stochastic	deterministic

Table 1: **Model comparison of ABM and PDMM.** The term $\mathcal{O}(n_a)^*$ describes the runtime scaling due to transition rates and can be replaced by $\mathcal{O}(1)$ under the assumption that spatial transitions are several orders of magnitude lower than infection state adoptions.

2.4.1. Spatial Hybridization

The general concept of the spatial hybridization has already been introduced in Section 2.2. In the following, we will provide some further details on the precise realization. Assume Ω_1 to be the focus region. For the precise implementation, ABM and PDMM are set up for the whole domain while both models have no movement or infection state adoptions in the nonrelevant regions meaning the focus region for the PDMM and all regions outside the focus regions for the ABM, i.e. the corresponding rates are zero. Then, both models are run independently from each other as long as no agents are leaving or entering the focus region. On time points for population exchange, models will be synchronized. The basic implementation idea shown in Algorithm 1.

As mentioned before, the exchange of agents and populations between the models is a crucial aspect of the hybridization. As the mobility process of the PDMM is also based on agents and not on shares of the whole population, we always exchange agents between both models. The exchange between ABM and PDMM is then done as follows:

- ABM \rightarrow PDMM: As we switch from fine-granular to a corresponding coarse-granular model, the exchange can be done by a trivial projection. Out-commuting agents from the focus region Ω_1 are just added to the subpopulation $N_i^{(k)}$ in the PDMM according to their updated position $x \in \Omega_k, k = 2, \dots, n_R$ and infection state $i \in \mathcal{Z}$. Subsequently, this agent is removed from the ABM.

Algorithm 1: Spatial hybridization

- 1 Create ABM and PDMM for $\Omega = \bigcup_{k=1}^{n_R} \Omega_k$ and $t = t_0$;
- 2 Set and restrict rates and populations;
- 3 ABM for Ω_1 ;
- 4 PDMM for $\Omega_2, \dots, \Omega_{n_R}$;
- 5 **While** $t \in [t_0, t_{max}]$ **do**;
- 6 Define next synchronization point \hat{t} ;
- 7 Advance ABM and PDMM from t to \hat{t} ;
- 8 Exchange populations;
- 9 Set $t = \hat{t}$;

- PDMM \rightarrow ABM: The exchange from coarse-granular to fine-granular is not as trivial as the PDMM only has information aggregated to region and compartment. It misses concrete positions inside the subregions. For the corresponding models, all infection state information can be taken from the corresponding subpopulation compartment. For the position, we do an educated guess and the new position is sampled from an appropriate distribution. The distribution depends on the distinct behavior of the ABM movement operator L , see (9).

To get the initial populations for the spatial-hybrid model, we only add agents to the ABM and then make one exchange step to set the initial system state $N(0)$ in the PDMM. With this, all agents outside Ω_1 are removed from the ABM, and in the PDMM the population in Ω_1 is set to 0.

2.4.2. Temporal Hybridization

The setup for the temporal-hybrid model is similar to the implementation of the spatial hybridization described in Section 2.4.1, in so far as both models are setup with matching parameters and used on the whole domain. However, instead of restricting the models spatially, only one model runs at a time. To decide which model that is, we define a function Γ that returns, based on time and the system state at t and predefined criteria, a model $\{\text{ABM}, \text{PDMM}\}$, i.e., Γ is a function that determines with which model to continue from a given time point. In the application presented in Section 3.2, the model choice depends on the number of infectious agents, which makes most sense as infectious disease dynamics are driven by the stochasticity in the behavior of infectious agents. The procedure is shown in Algorithm Algorithm 2.

Algorithm 2: Temporal hybridization

```
1 Create ABM and PDMM for  $\Omega$  at  $t = t_0$ ;  
2 Select one model as  $m_{current}$ ;  
3 Initialize population only for  $m_{current}$ ;  
4 Define time step  $\Delta t$ ;  
5 While  $t \in [t_0, t_{max}]$  do;  
6    $m_{next} = \Gamma(m_{current}, t)$ ;  
7   If  $m_{current} \neq m_{next}$ ;  
8     Move the population from  $m_{current}$  to  $m_{next}$ ;  
9      $m_{current} = m_{next}$ ;  
10  Set  $t = t + \Delta t$ ;  
11  Advance  $m_{current}$  to  $t$ ;
```

Moving the population between the models follows the same principle as the agent exchange described in Section 2.4.1, applied to all agents in all regions at once.

3. Results

In this section, we provide simulation results for the standalone agent- and metapopulation-based models presented in Section 2.3. We will compare these results against our spatial- and temporal-hybrid models. All models are simulated using a temporal Gillespie algorithm, allowing us to obtain stochastically exact results without sampling the distribution [36, 37]. We will highlight differences and similarities in the particular model outcomes and compare model runtimes as a proxy indicator for computational effort. All simulations were conducted on a Intel Xeon "Skylake" Gold 6132 (2.60 GHz) with four nodes with 14 CPU cores each and 384GB DDR4 memory, using separate cores to conduct Monte Carlo runs in parallel.

3.1. Spatial Hybridization

In the following, we present the results for two applications of the spatial hybridization. The first application naturally extends the theoretical setting of [19] by using four instead of two potential wells (i.e. local minima of the potential) and significantly more agents. In the second application, we consider a more realistic setting with the city of Munich and its surrounding counties.

3.1.1. Application 1 - A mathematical quadwell example

In this section, we naturally extend the double-well example from [19] by considering a quadwell potential with a constant noise term $\sigma \in \mathbb{R}$. The quadwell potential is given by

$$F(x, y) = (x^2 - 1)^2 + (y^2 - 1)^2; \quad (16)$$

see Fig. 3. The magnitude of the noise term determines the number of transitions between metaregions, see Fig. 4.

We define the focus region as the upper left quadrant defined by $(-\infty, 0) \times (0, \infty)$. We number the wells in Fig. 3b from 1 to 4 starting with the upper left, focus well and ending with the lower right well, numbered line by line. We simulate the ABM, the PDMM and the spatial-hybrid model for $t_{max} = 150$ days. We choose $n_a = 8000$ agents with 1% of the population being initially infected in every well (0.2% Exposed, 0.3% Carrier and 0.5% Infected). The transmission probability $\rho^{(k)}$ is the same in all regions apart from region 2 which has a transmission probability three times higher than the other regions. All parameters and their values are given in Table B.4, motivated by [10]. However, as the scope of the current paper is the disease-agnostic introduction of novel hybrid models, no further parameter refinement for COVID-19 has been performed. The results of 500 simulations are shown in Fig. 5. Comparing Fig. 5b and Fig. 5c, it can be seen that region 2 is the main driver of the infection dynamics and that for a high number of infected agents, the PDMM approximates the ABM outcomes sufficiently well. As region 2 is not the focus region, this region is modeled with the PDMM in the spatial-hybrid, therefore the PDMM and hybrid model curves

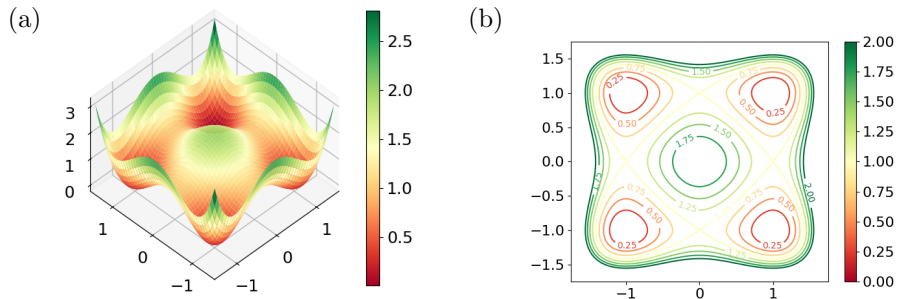


Figure 3: **Quadwell potential (16) used for the diffusion process in the ABM.** The four metaregions are separated by the axes $x = 0$ and $y = 0$. The figure shows an (a) isometric view and (b) a contour plot of the potential.

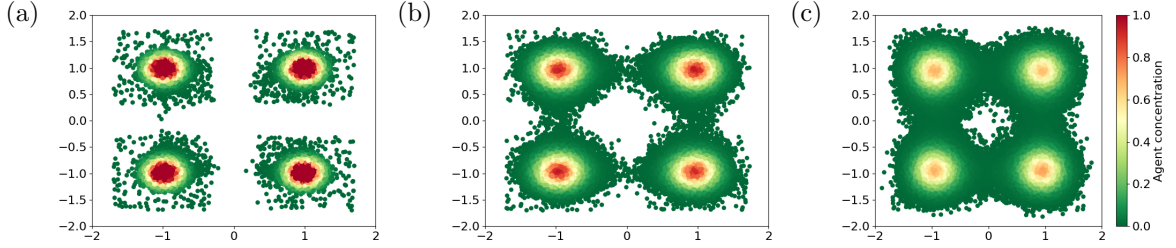


Figure 4: **Position distribution for a simulation of 800 agents for 50 days in the quadwell scenario.** Results for noise term (a) $\sigma = 0.3$, (b) $\sigma = 0.5$ and (c) $\sigma = 0.6$. Agents are initialized with positions having 0.3 distance from the axes with $x = 0$ and $y = 0$.

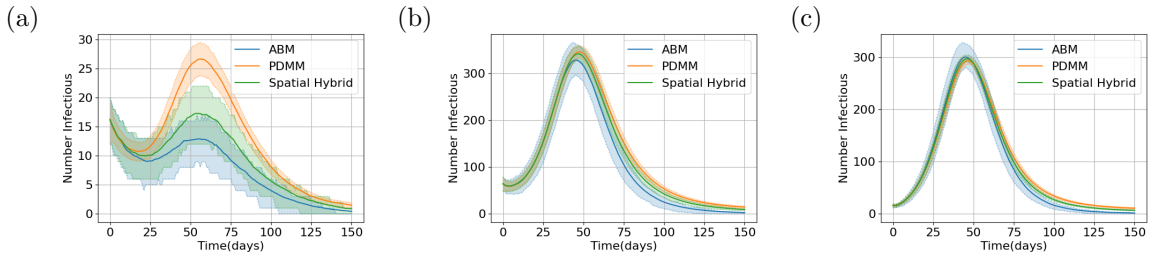


Figure 5: **Spatial hybridization for the quadwell potential: Focus region, sum of all regions and Region 2.** Number of infectious agents (compartments C and I) for (a) the focus region (b) the sum of all regions and (c) Region 2. The figures show the mean outcomes in solid lines with a partially transparent face between the p25 and p75 percentiles from 500 runs.

are almost overlapping. Fig. 5a shows that in the focus region the hybrid model fits the ABM outcomes much better than the PDMM. For the sake of completeness, the results for region 2 and region 3 are shown in Fig. A.12.

The runtime of the spatial-hybrid model is dominated by the ABM, but is still one order of magnitude smaller than the ABM runtime for 400 agents and even two orders of magnitude for 16,000 agents, see Fig. 6a. For 40,000 agents, the runtime for the described scenario can be reduced by 98% using the spatial-hybrid model.

3.1.2. Application 2 - Infectious disease spread in Munich and surrounding counties.

Secondly, we want to consider a more realistic application, in particular an application for the city of Munich, defined as our focus region, and its

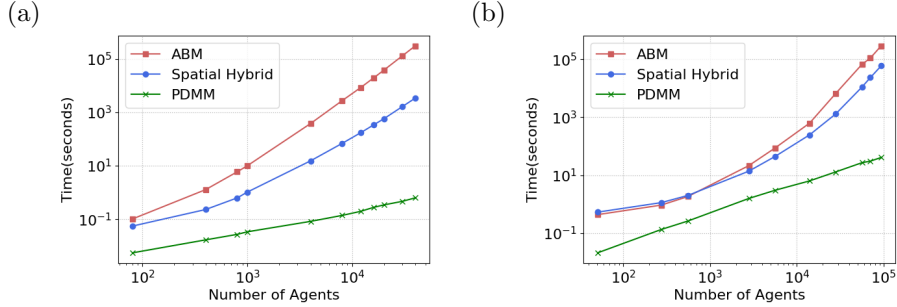


Figure 6: **Log-scaled runtime (in seconds) for ABM, PDMM and spatial-hybrid model.** Results for (a) the quadwell example with the setup according to Table B.4 and (b) the scenario of the city of Munich with setup according to Table B.5.

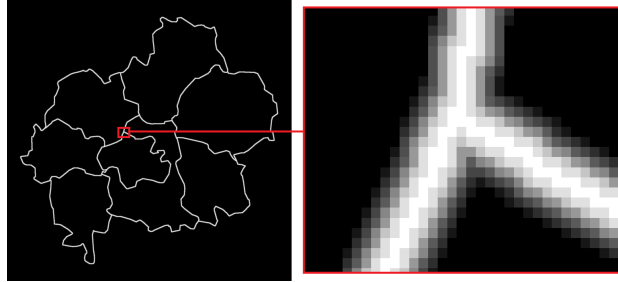


Figure 7: **Potential defined for the ABM in and around Munich.** Black areas have value 0 and white parts value 1. We obtain the potential F by discretizing the map, resulting in a matrix $P \in [0, 1]^{p \times p}$ and then interpolating between matrix entries.

surrounding counties.

To realize realistic intercounty mobility patterns, we define a potential on the political map of the considered counties. We apply a Gaussian curve on the discretized (in pixels) county borders to define a potential $F(x)$. More precisely, $F(x) = h$ if x is on a border, $F(x) \in (0, h)$ modeled through a Gaussian curve if x is in a given distance from the border and $F(x) = 0$ otherwise, i.e., inside a county. The resulting potential directly determines eight regions for the PDMM, aligning with the eight counties considered. Fig. 7 shows the potential with a zoomed in snippet to the gradient on the border. For this potential the noise term σ and the border height h determines the time scale for an agent crossing a border. A drawback of modeling agent movements with potential and diffusion process is the limited control on intercounty mobility, in particular that only agents next to the borders can transition to neighboring regions in an appropriate time. However, in reality

individuals that are further away from the borders should also transition to neighboring counties in a moderate time, e.g., on a daily basis caused by commuting activities. To that end we modify the agents' movements. For short-distance travel, we use the movement operator L given by Eq. (10), where we set the border height h for the potential F to 10 and additionally prevent crossing borders through random walks. For long-distance travel, we introduce two normally distributed random variables T_d^α and T_r^α for agent α . Samples of these variables are only used when α is a commuter on the current day $\lfloor t \rfloor$. We use the random variable $T_d^\alpha \sim \mathcal{N}(\mu_d, \sigma_d)$ for the time point an agent α leaves its home county on day $\lfloor t \rfloor$ and $T_r^\alpha \sim \mathcal{N}(\mu_r, \sigma_r)$ the time point an agent α returns on day $\lfloor t \rfloor$ – ignoring and resampling values beyond three standard deviations to ensure that samples are in $[0, 1]$. We introduce a commuting term $K(t)$, which is added onto L , which allows us to better control the desired number of border crossings. Let $K_\alpha(t)$ be the α -th component of $K(t)$, that is zero if agent α is not a commuter on day $\lfloor t \rfloor$. If α is a commuter, $K_\alpha(t)$ is given by

$$K_\alpha(t) = \begin{cases} \pi(x_\alpha) - x_\alpha, & \text{if } t_d^\alpha + \lfloor t \rfloor \in (t, t + \delta t] \vee t_r^\alpha \in (t, t + \delta t] \\ 0, & \text{else} \end{cases}, \quad (17)$$

where $\lfloor t \rfloor$ marks the beginning of the day and t_d^α and t_r^α are realizations of T_d^α and T_r^α . Furthermore, $\pi : \Omega \rightarrow \Omega$ is a random variable on the domain using the probability function

$$\mathbb{P}(\pi(x_\alpha) = y) = \mathbb{P}(y | x_\alpha \in \Omega_k; y \in \Omega_l) \cdot \lambda^{(k,l)} = \begin{cases} \frac{\lambda^{(k,l)}}{\nu(\Omega_l)}, & l \neq k \\ \lambda^{(k,k)}, & l = k \wedge x_\alpha = y \\ 0, & l = k \wedge x_\alpha \neq y \end{cases}, \quad (18)$$

where $\lambda^{(k,l)}$ is the relative number of commuters from region Ω_k to region Ω_l and ν a counting measure on the discretized map (see Fig. 7) ignoring border pixels. Hence $\nu(\Omega_l)$ is the number of pixels inside region Ω_l . When using this adapted movement for the ABM, we need to adapt the exchange of agents from PDMM to ABM for the spatial-hybrid as well. When we exchange an agent α from PDMM to ABM, we (uniformly) sample a new position for it in the focus region. Depending on the current time t , we decide whether the agent has started its commute or is returning from it. In case of the former, i.e., if $t \leq \lfloor t \rfloor + \mu_d + \sigma_d$, a return time t_r^α is drawn. Fig. 8 shows that through

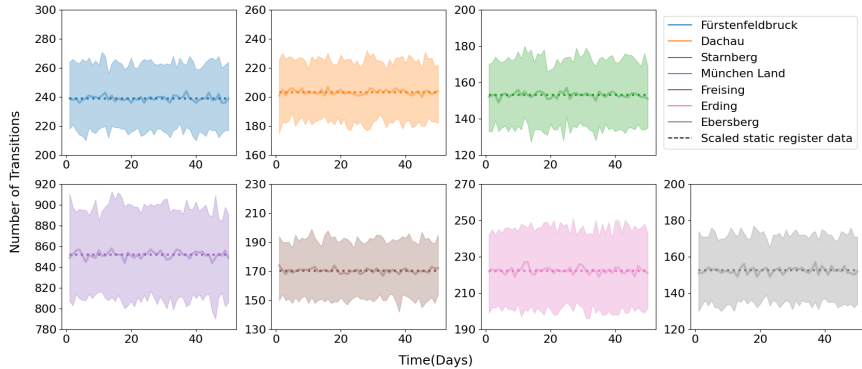


Figure 8: **Daily commuting from and to Munich City for different surrounding counties.** 5% and 95% percentiles of daily transitions in simulations shown as colored area together with median as solid line. The static register data from Federal Agency of Work, scaled to number of simulated agents, is shown as dotted lines.

the incorporation of the commuting term K , the number of daily transitions in Munich matches the static daily commuting data scaled according to the number of agents n_a .

In our focus region, Munich City, we initialize $n_a = 14,064$ agents. We only have initially infected agents (0.05% Exposed, 0.05% Carrier and 0.1% Infected) in Munich (Landkreis), which is the region directly neighboring Munich City in North, East and South. In all other regions, all agents are Susceptible at the beginning. All parameters and their values for this application are shown in Table B.5. We run the simulations for $t_{max} = 50$ days. We note that the PDMM mean fits the ABM mean better than in the quadwell potential, see Fig. 9. As a result, the spatial-hybrid also delivers a better fit to the ABM for both, the focus region and the sum of all regions. While on first glance, the PDMM and its median outcome approaches the ABM quite well, its limitations lie in the percentile outcomes. Looking at the percentiles, it can be observed that in 25% of the ABM runs, no infected agents enter the focus region. The PDMM is not able to capture these dynamics. On the other hand, the 25% prediction interval of the spatial-hybrid model can capture this effect until day 35.

The runtime gain for the Munich potential is smaller than in the quadwell potential but the spatial-hybrid model is still 5-times faster than the ABM for 93,000 agents, which is a runtime gain of 80%, see Fig. 6b. The reason for this

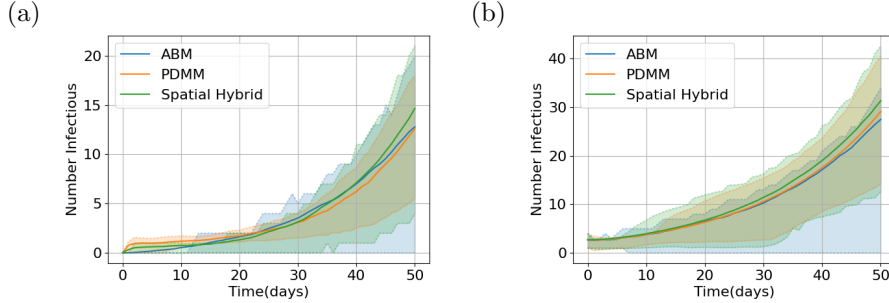


Figure 9: **Spatial hybridization for the Munich City example: Focus region and sum of all regions.** Number of infectious agents (compartments C and I) for (a) Munich City (focus region) and (b) the sum of all regions. The figures show the mean outcomes in solid lines with a partially transparent face between the p25 and p75 percentiles from 500 runs.

reduced effect is the very disadvantageous setup for the hybrid model with Munich City as focus region, because its population makes up approximately 75% of all agents in the modeled counties. Consequently, in the spatial-hybrid model, the number of agents modeled with the ABM is roughly 75% of n_a while in the quadwell potential it is only 25% of all agents. Secondly, the chosen initialization also has a relevant influence on the runtime gain. As we have a very low number of infectious agents in the simulation (at most 0.28% of the total population compared to approximately 3.75% in the quadwell), there are only a few infection state adoptions in the ABM per time step, which leads to less computational costs. One can observe that the runtime for the spatial-hybrid model for Munich is even slightly higher than the ABM runtime for $n_a < 600$. This can again be explained by the percentage of agents in the focus region compared to the whole domain and the relatively low runtime of the ABM due to very low numbers of infectious agents. Therefore the exchange of agents from PDMM to ABM - which is slightly more complex for the Munich potential compared to the quadwell potential - produces overhead which only amortized for $n_a > 600$.

3.2. Temporal hybridization

For the temporal hybridization we consider a single well potential given by

$$F(x, y) = \frac{x^4 + y^4}{2}, \quad (19)$$

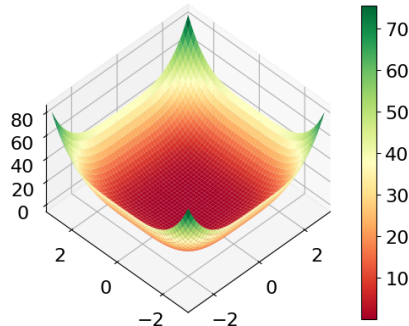


Figure 10: **Single well potential (19) used for the diffusion process in the ABM of the temporal-hybrid model.**

see Fig. 10. By design we only have one region and the PDMM reduces to a classical ODE-based model without spatial transitions. We use a constant noise $\sigma \in \mathbb{R}$ for the diffusion process and a relatively small contact radius r , thus σ has a crucial influence on contacts between agents in the ABM and consequently on second-order adoptions. Again, we use the adoption model from Fig. 2. All parameters and their values for the single well application are listed in Table B.6.

We choose a scenario with exactly one infected agent in compartment I with an otherwise susceptible population. The transmission probability ρ is set such that in around 30% of all simulations, the virus dies out. Otherwise, we get an epidemic outbreak and introduce a nonpharmaceutical intervention (NPI) which is implemented through a reduction of ρ by 80% after $t_{NPI} = 0.5(t_0 + t_{max})$. This NPI then leads to a slow decline of infections over the remaining parts of the simulation.

Since we are considering only one region, the derived PDMM is a deterministic ODE model in which the virus never dies out. Obviously, we cannot use this PDMM to meaningfully simulate this specific scenario in its entirety. However, we can use the PDMM to speed up calculation once an outbreak reaches a certain size or after the virus has become extinct. Therefore, the temporal-hybrid model always starts with the ABM, and then switches to the PDMM once an extinction or an outbreak reaches a certain size. The latter is defined by a threshold $s > 1$ to be compared against the sum of agents in infection states E , C and I . If this number is larger than s , we switch the model to the PDMM, projecting the whole population of the ABM. A suitable value for the threshold s depends on the specific setup, especially on

the transmission probability ρ . It is not trivial to determine particularly for real-world scenarios.

A second threshold $0 \leq s' < s$ could be introduced to switch from PDMM to ABM as soon as the number of infected agents falls below s' . This second threshold indicates a number of infected, where stochasticity is (again) important to determine the development of the disease dynamics. This can be of particular importance if disease mitigation, e.g., through NPIs, had been conducted successfully. In the presented scenario, we simply set s' to zero.

Here, the model selection function Γ from Algorithm 2 returns the PDMM if the number of infected agents exceeds s , and the ABM otherwise. We choose $t_0 = 0$, $t_{max} = 40$, and a fixed step size of $\Delta t = 0.2$ for this Algorithm. The single initially infected agent is chosen randomly from the entire population. Fig. 11 shows the results of 10,000 simulations of ABM, PDMM and the temporal-hybrid with $s = 2$ and $s = 5$ in form of the mean result as well as the 25th- and 75th-percentile for the stochastic models.

The reduction of ρ at $t_{NPI} = 20$ leads to a kink in the number of infected agents (compartments E , C and I), see Fig. 11a. Since in 30% of all ABM simulations the virus dies out, the 25th-percentile is almost entirely zero, except for right after the initialization. We can also see that the percentiles as well as the means of the temporal-hybrid models with $s = 2$ and $s = 5$ are fairly close together, hence they are both good approximations to the pure ABM. As the PDMM is deterministic, the percentiles and means of it are all the same and are close to the ABM mean. While Fig. 11a shows the results for all simulations, Fig. 11b shows mean, p25 and p75 for all simulations where the virus becomes extinct and Fig. 11c the corresponding curves for all simulations where the virus survives, hence an outbreak occurs. The PDMM is not shown in Fig. 11b as it is not able to capture the extinction scenario. In Fig. 11c both temporal-hybrid models and ABM curves have shifted upwards compared to the results of all simulations in Fig. 11a. The PDMM result remains trivially the same and therefore underestimates the mean number of infected in the survival scenarios, see Fig. 11c. For completeness, we also provide the results for the later compartment I , see ??, in the appendix, where we see a rather smooth transition compared to the kink in Fig. 11. Both switching thresholds seem to be a good choice as the resulting temporal-hybrid models are very close to the ABM results - the mean as well as the percentiles. Note, however, that the low thresholds are due to a large transmission probability ρ and dense contact network realized through the diffusion-drift process. In Fig. 11b, the mean of the temporal-hybrid

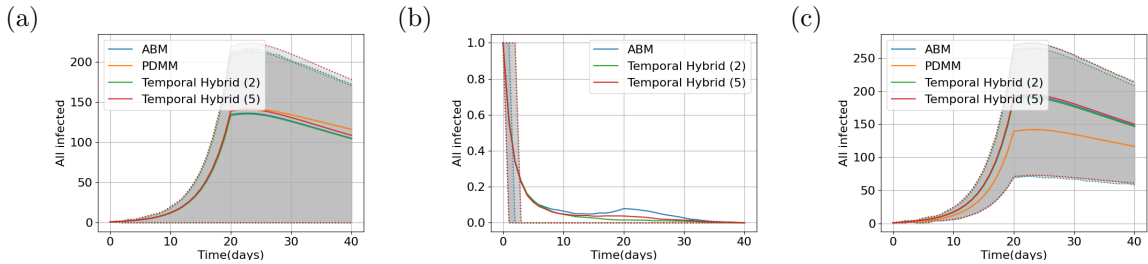


Figure 11: **Temporal hybridization for the single well example and number of infected agents in compartments E , C , and I .** The subfigures show (a) all runs, (b) extinction runs with virus extinction, and (c) survival runs without virus extinction for ABM, PDMM and temporal-hybrid models with $s = 2$ and $s = 5$. The figures show the mean outcomes in solid lines with a partially transparent face between the p25 and p75 percentiles from 10,000 runs with 10,000 agents.

model with $s = 5$ is a little closer to the ABM mean, but both mean hybrid model outcomes from the extinction simulations do not capture the increase of the ABM mean until t_{NPI} . The reason for that is that the temporal-hybrid models switch to a PDMM if the number of infected is high enough, thus these models are then not be able to produce an extinction scenario anymore.

The ABM runs significantly faster in extinction runs than in survival runs (see Table 3), as there are no pairwise interactions to consider once there are no infected agents anymore. Furthermore, the PDMM is - as expected - multiple orders of magnitude faster than the ABM, making it desirable to use it whenever possible. On average, the temporal-hybrid model for both values of s is almost three times faster than the ABM in the results for all simulations (see Table 2) almost two times for the extinction simulations (see Table 3), and more than three times for the survival simulations (see Table 3). When comparing the total simulation time for the different switching thresholds, all survival simulations show a time gain when using the lower threshold of $s = 2$. Otherwise, the timings for both thresholds are very similar. For all stochastic models (ABM and temporal-hybrid), the difference in minimum and maximum time to the mean time correlates with the large variation in simulation outcomes; see the percentiles in Fig. 11. For this application, we do not further examine the runtime scaling behavior, as it does not behave significantly different to the results for the spatial-hybrid model, see Section 2.4 and Fig. 6. The runtime of the temporal-hybrid model is dominated by the proportion of time (instead of population) in which the ABM is used for the simulation.

Model	All simulations		
	min	mean	max
<i>ABM</i>	80.94	344.30	2091.56
<i>PDMM</i>	0.00040	0.00046	0.01000
<i>Temporal-hybrid</i> $s = 2$	42.33	116.26	634.26
<i>Temporal-hybrid</i> $s = 5$	42.31	120.05	655.27

Table 2: Summarized simulation (in sec) timings for ABM, PDMM and temporal-hybrid models for all 10,000 simulations.

Model	Extinction simulations			Survival simulations		
	min	mean	max	min	mean	max
<i>ABM</i>	80.94	93.01	112.66	93.18	446.24	2091.56
<i>PDMM</i>	-	-	-	0.00040	0.00046	0.01000
<i>Temporal-hybrid</i> $s = 2$	42.33	48.79	99.75	45.09	143.97	634.26
<i>Temporal-hybrid</i> $s = 5$	42.31	49.37	102.76	46.02	147.47	655.27

Table 3: Summarized simulation timings (in sec) for ABM, PDMM and temporal-hybrid models for simulations with and without virus extinction.

4. Discussion and Conclusion

While the number of research articles on hybrid models in the sense of our understanding is very small, several authors have published pioneering works in [28, 27, 26, 25, 29] over the last two decades. The approaches coming closest to our works are given in [28, 29]. However, run time and computational cost has, e.g., not been considered in [28]. In [29] various interesting results have been published for a model running on a laptop computer.

In this work, we formalized two hybridization approaches and introduced a general framework of spatial and temporal hybrid models, combining agent-based and equation- or metapopulation-based models. In particular, the temporal-hybrid model is also an *adaptive* model and future works may also consider adaptivity in time and space through spatio-temporal hybrid models.

We here further presented two suitable models recently introduced, which were adapted for our examples and combined in the suggested manner. The critical aspect of combining these models is the definition of exchange rules, an issue that has not been discussed a lot yet but which has an essential impact on the accuracy and the performance of the hybridization. Models that

are derived from one another in a theoretical way, like in [19, 38] offer a more direct way to implement exchanges. Nevertheless, nuances in projections or mappings can become important as it has been observed in our simulations. With the presented random walk movement of agents, the same agent may cross region boundaries multiple times in a short time, which might drastically change the hybrid model’s outcome compared to the outcome of the fine model if this effect is not accounted for in the coarse model.

The movement pattern of the ABM, given by a potential and a Brownian motion is a rather theoretical movement pattern that delivered us two suitable models to be combined. In future work, we will investigate other agent-based models realizing discrete locations such as schools or workplaces. For these, more sophisticated methods for projection and, also, reconstruction of information might be needed.

As shown, hybrid models can combine the best of both worlds and deliver fine-granular insights through the use of ABMs, only using modest or substantially reduced computational resources. Both hybridization approaches were able to capture disease dynamics of the ABM better than the PDMM. For the quadwell potential, the fitting of the PDMM to the ABM could be improved by better parameter estimation, e.g., through making the spatial transition rates dependent on time and infection state. This would then also bring ABM and hybrid model results closer together.

For the spatial hybridization, the runtime gain depends on the total number of agents in the focus region, relative to all other regions modeled by equations. Similarly, the temporal hybridization runtime gain depends mostly on the proportion of simulation time that the ABM is used. From our simulations, we have seen that up to 98 % of the simulation time can be saved by replacing an ABM by a spatial-hybrid model. Although this number depends highly on the chosen models and the individual setting, a reduction of 90 % of the simulation time or a speedup of 10 can be achieved easily.

Acknowledgments

The authors JB and MJK have received funding by the German Federal Ministry of Education and Research under grant agreement 031L0297B (Project INSIDe). RS and MJK have received funding by the German Federal Ministry for Digital and Transport under grant agreement FKZ19F2211A (Project PANDEMOS), RS has received funding by the German Federal Ministry for Digital and Transport under grant agreement FKZ19F2211B

(Project PANDEMOS). MJK has received funding from the Initiative and Networking Fund of the Helmholtz Association (grant agreement number KA1-Co-08, Project LOKI-Pandemics).

Competing interests

The authors declare to not have any competing interests.

Data availability

The MEmilio code repository is publicly available on Github under <https://github.com/SciCompMod/memilio>, the developed models are to be found on the fork release <https://github.com/reneSchm/memilio/releases/tag/hybrid-paper> (based on the branch hybrid-model-omp); The models can be found in the directory /cpp/hybrid_paper, with simulation algorithms under /cpp/models/mpm. All input data can be generated with or is in the code repository. Visualized simulation data can be shared upon request.

Author Contributions

Conceptualization: Julia Bicker, René Schmieding, Martin Kühn

Data Curation: Julia Bicker, René Schmieding

Formal Analysis: Julia Bicker, René Schmieding, Martin Kühn

Funding Acquisition: Martin Kühn, Michael Meyer-Hermann

Investigation: Julia Bicker, René Schmieding, Martin Kühn

Methodology: Julia Bicker, René Schmieding, Martin Kühn

Project Administration: Martin Kühn

Resources: Martin Kühn, Michael Meyer-Hermann

Software: Julia Bicker, René Schmieding

Supervision: Martin Kühn, Michael Meyer-Hermann

Validation: All authors

Visualization: Julia Bicker, René Schmieding

Writing – Original Draft: Julia Bicker, René Schmieding, Martin Kühn

Writing – Review & Editing: All authors

Appendix A. Supplementary Figures

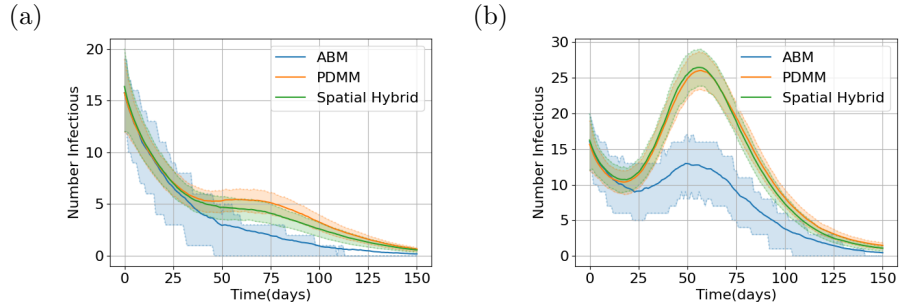


Figure A.12: **Spatial hybridization for the quadwell potential: Region 3 and 4.** Number of infectious agents (compartments C and I) for (a) Region 3 and (b) Region 4. The figures show the mean outcomes in solid lines with a partially transparent face between the p25 and p75 percentiles from 500 runs.

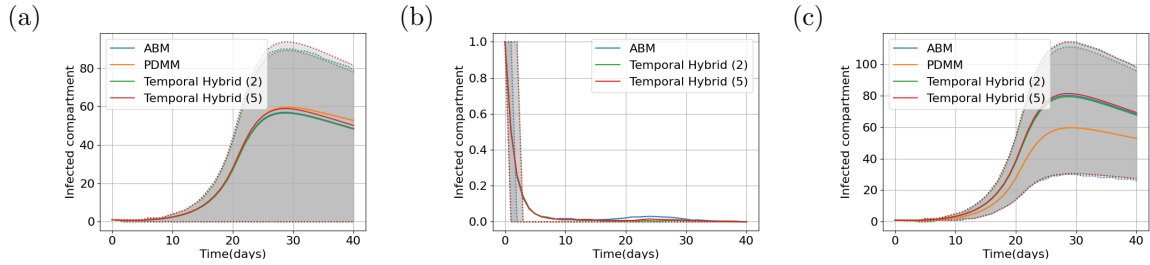


Figure A.13: **Temporal hybridization for the single well example and number of agents in compartment Infected.** (a) All runs and selected runs (b) with and (c) without virus extinction for ABM, PDMM and temporal-hybrid models with $s = 2$ and $s = 5$. The figures show the mean outcomes in solid lines with a partially transparent face between the p25 and p75 percentiles from 10,000 runs with 10,000 agents.

Appendix B. Supplementary Tables

Parameter	Description	Value
n_a	Number of agents	8000
ρ	Transmission probability. As it is region dependent it is given as vector $(\rho^{(0)}, \rho^{(1)}, \rho^{(2)}, \rho^{(3)})$.	(0.1, 0.3, 0.1, 0.1)
$\xi_C^{(k)}$	Increase or decrease factor on transmission probability for Carrier	1.0
$\xi_I^{(k)}$	Increase or decrease factor on transmission probability for Infected	1.0
$\gamma_{E,C}^{(k)}$	Rate from Exposed to Carrier. Is equal to $\frac{1}{T_E}$ with T_E the average time of an agent being in the exposed state.	$\frac{1}{3}$
$\gamma_{C,R}^{(k)}$	Rate from Carrier to Recovered	$\frac{1}{30}$
$\gamma_{C,I}^{(k)}$	Rate from Carrier to Infected	$1 - \gamma_{C,R}^{(k)}$
$\gamma_{I,D}^{(k)}$	Rate from Infected to Dead	0.0008
$\gamma_{I,R}^{(k)}$	Rate from Infected to Recovered	$1 - \gamma_{I,D}^{(k)}$
r	Interaction radius	0.4
σ	Noise term of the diffusion process	0.55
$\lambda_i^{(k,l)}$	Spatial transition rates	0 for $i = D$; for $i \in \mathcal{Z} \setminus D$: 0.0048 for laterally adjacent regions, $1e^{-7}$ for diagonally adjacent regions

Table B.4: Parameter choices for the spatial hybridization scenario of the quadwell potential.

Parameter	Description	Value
n_a	Number of agents	14064
$\rho^{(k)}$	Transmission probability.	0.2
$\xi_C^{(k)}$	Increase or decrease factor on transmission probability for Carrier	1.0
$\xi_I^{(k)}$	Increase or decrease factor on transmission probability for Infected	1.0
$\gamma_{E,C}^{(k)}$	Rate from Exposed to Carrier. Is equal to $\frac{1}{T_E}$ with T_E the average time of an agent being in the exposed state.	$\frac{1}{3}$
$\gamma_{C,R}^{(k)}$	Rate from Carrier to Recovered	$\frac{2}{30}$
$\gamma_{C,I}^{(k)}$	Rate from Carrier to Infected	$1 - \gamma_{C,R}^{(k)}$
$\gamma_{I,D}^{(k)}$	Rate from Infected to Dead	0.0005
$\gamma_{I,R}^{(k)}$	Rate from Infected to Recovered	$1 - \gamma_{I,D}^{(k)}$
r	Interaction radius in km	50
σ	Noise termin of the diffusion process	10
$\lambda_i^{(k,l)}$	Spatial transition rates	Correspond to entries of commuter matrix for $i \neq D$, and are zero for $i = D$
μ_d	Mean of commuting agents depart time	$\frac{9}{24}$
σ_d	Standard deviation of commuting agents depart time	$\frac{4}{24}$
μ_r	Mean of commuting agents return time	$\frac{18}{24}$
σ_r	Standard deviation of commuting agents depart time	$\frac{5}{24}$

Table B.5: Parameter choices for the spatial hybridization for the Munich potential.

Parameter	Description	Value
n_a	Number of agents	10,000
ρ	Transmission probability	0.6 initially, 0.12 after t_{npi}
$\xi_C^{(k)}$	Increase or decrease factor on transmission probability for Carrier	1.0
$\xi_I^{(k)}$	Increase or decrease factor on transmission probability for Infected	1.0
$\gamma_{E,C}^{(k)}$	Rate from Exposed to Carrier. Is equal to $\frac{1}{T_E}$ with T_E the average time of an agent being in the exposed state.	$\frac{1}{3}$
$\gamma_{C,R}^{(k)}$	Adoption rate from Carrier to Recovered	$\frac{1}{30}$
$\gamma_{C,I}^{(k)}$	Adoption rate from Carrier to Infected	$1 - \gamma_{C,R}^{(k)}$
$\gamma_{I,D}^{(k)}$	Adoption rate from Infected to Dead	0.0008
$\gamma_{I,R}^{R,(k)}$	Adoption rate from Infected to Recovered	$1 - \gamma_I^{D,(k)}$
r	Interaction radius, fairly small compared to the other models	0.1
σ	Noise term of the diffusion process	0.5

Table B.6: Parameter choices for the temporal hybridization using a single well potential.

References

- [1] T. V. Callaghan, F. Bergholm, T. R. Christensen, C. Jonasson, U. Kokfelt, M. Johansson, A new climate era in the sub-Arctic: Accelerating climate changes and multiple impacts, *Geophysical Research Letters* 37 (14) (2010) 2009GL042064. doi:10.1029/2009GL042064.
URL <https://agupubs.onlinelibrary.wiley.com/doi/10.1029/2009GL042064>
- [2] P. Daszak, J. Amuasi, C. das Neves, D. Hayman, T. Kuiken, B. Roche, C. Zambrana-Torrel, P. Buss, H. Dunderova, Y. Feferholtz, et al., Workshop Report on Biodiversity and Pandemics of the Intergovernmental Platform on Biodiversity and Ecosystem Services (IPBES), Tech. rep. (Oct. 2020).
URL <https://doi.org/10.5281/zenodo.7432079>
- [3] P. R. Epstein, Climate change and emerging infectious diseases, *Microbes and Infection* (2001).
- [4] R. C. Reiner, R. M. Barber, J. K. Collins, P. Zheng, C. Adolph, J. Albright, C. M. Antony, A. Y. Aravkin, S. D. Bachmeier, B. Bang-Jensen, IHME COVID-19 Forecasting Team, et al., Modeling COVID-19 scenarios for the United States, *Nature Medicine* (2020) 1–12doi: 10.1038/s41591-020-1132-9.
- [5] C. C. Kerr, R. M. Stuart, D. Mistry, R. G. Abeysuriya, K. Rosenfeld, G. R. Hart, R. C. Núñez, J. A. Cohen, P. Selvaraj, B. Hagedorn, L. George, M. Jastrzebski, A. S. Izzo, G. Fowler, A. Palmer, D. Delport, N. Scott, S. L. Kelly, C. S. Bennette, B. G. Wagner, S. T. Chang, A. P. Oron, E. A. Wenger, J. Panovska-Griffiths, M. Famulare, D. J. Klein, Covasim: An agent-based model of COVID-19 dynamics and interventions, *PLOS Computational Biology* 17 (7) (2021) 1–32, publisher: Public Library of Science. doi:10.1371/journal.pcbi.1009149.
URL <https://doi.org/10.1371/journal.pcbi.1009149>
- [6] W. Koslow, M. J. Kühn, S. Binder, M. Klitz, D. Abele, A. Basermann, M. Meyer-Hermann, Appropriate relaxation of non-pharmaceutical interventions minimizes the risk of a resurgence in SARS-CoV-2 infections in spite of the Delta variant, *PLOS Computational Biology* 18 (5) (2022)

e1010054. doi:10.1371/journal.pcbi.1010054.

URL <https://dx.plos.org/10.1371/journal.pcbi.1010054>

- [7] M. J. Kühn, D. Abele, S. Binder, K. Rack, M. Klitz, J. Kleinert, J. Gilg, L. Spataro, W. Koslow, M. Siggel, M. Meyer-Hermann, A. Basermann, Regional opening strategies with commuter testing and containment of new SARS-CoV-2 variants in Germany, *BMC Infectious Diseases* 22 (1) (2022) 333. doi:10.1186/s12879-022-07302-9.
URL <https://bmcinfectedis.biomedcentral.com/articles/10.1186/s12879-022-07302-9>
- [8] J. P. Medlock, *Integro-differential-equation models in ecology and epidemiology*, University of Washington, 2004.
- [9] J. Liu, G. P. Ong, V. J. Pang, Modelling effectiveness of COVID-19 pandemic control policies using an Area-based SEIR model with consideration of infection during interzonal travel, *Transportation Research Part A: Policy and Practice* 161 (2022) 25–47. doi:10.1016/j.tra.2022.05.003.
URL <https://linkinghub.elsevier.com/retrieve/pii/S0965856422001197>
- [10] M. J. Kühn, D. Abele, T. Mitra, W. Koslow, M. Abedi, K. Rack, M. Siggel, S. Khailaie, M. Klitz, S. Binder, L. Spataro, J. Gilg, J. Kleinert, M. Häberle, L. Plötzke, C. D. Spinner, M. Stecher, X. X. Zhu, A. Basermann, M. Meyer-Hermann, Assessment of effective mitigation and prediction of the spread of SARS-CoV-2 in Germany using demographic information and spatial resolution, *Mathematical Biosciences* (2021) 108648doi:<https://doi.org/10.1016/j.mbs.2021.108648>.
URL <https://www.sciencedirect.com/science/article/pii/S0025556421000845>
- [11] A. Bershteyn, J. Gerardin, D. Bridenbecker, C. W. Lorton, J. Bloedow, R. S. Baker, G. Chabot-Couture, Y. Chen, T. Fischle, K. Frey, et al., for the Institute for Disease Modeling, Implementation and applications of EMOD, an individual-based multi-disease modeling platform, *Pathogens and Disease* 76 (5) (Jul. 2018). doi:10.1093/femspd/fty059.
URL <https://academic.oup.com/femspd/article/doi/10.1093/femspd/fty059/5050059>

- [12] S. A. Müller, M. Balmer, W. Charlton, R. Ewert, A. Neumann, C. Rakow, T. Schlenker, K. Nagel, Predicting the effects of COVID-19 related interventions in urban settings by combining activity-based modelling, agent-based simulation, and mobile phone data, medRxiv (2021). doi:10.1101/2021.02.27.21252583.
- [13] J. Bracher, D. Wolfram, J. Deuschel, K. Görgen, J. L. Ketterer, A. Ullrich, S. Abbott, M. V. Barbarossa, D. Bertsimas, S. Bhatia, et al., A pre-registered short-term forecasting study of COVID-19 in Germany and Poland during the second wave, Nature Communications 12 (1) (2021) 5173. doi:10.1038/s41467-021-25207-0.
URL <https://www.nature.com/articles/s41467-021-25207-0>
- [14] G. P. Garnett, S. Cousens, T. B. Hallett, R. Steketee, N. Walker, Mathematical models in the evaluation of health programmes, The Lancet 378 (9790) (2011) 515–525. doi:10.1016/S0140-6736(10)61505-X.
- [15] L. Wynants, B. Van Calster, G. S. Collins, R. D. Riley, G. Heinze, E. Schuit, E. Albu, B. Arshi, V. Bellou, M. M. J. Bonten, et al., Prediction models for diagnosis and prognosis of covid-19: systematic review and critical appraisal, BMJ (2020) m1328doi:10.1136/bmj.m1328.
URL <https://www.bmj.com/lookup/doi/10.1136/bmj.m1328>
- [16] S. A. Müller, S. Paltra, J. Rehmann, K. Nagel, T. O. Conrad, Explicit modeling of antibody levels for infectious disease simulations in the context of SARS-CoV-2, iScience 26 (9) (2023) 107554. doi:10.1016/j.isci.2023.107554.
URL <https://linkinghub.elsevier.com/retrieve/pii/S2589004223016310>
- [17] L. Willem, S. Stijven, E. Tijssens, P. Beutels, N. Hens, J. Broeckhove, Optimizing agent-based transmission models for infectious diseases, BMC Bioinformatics 16 (1) (2015) 183. doi:10.1186/s12859-015-0612-2.
URL <https://bmcbioinformatics.biomedcentral.com/articles/10.1186/s12859-015-0612-2>
- [18] M. J. Kühn, J. Holke, A. Lutz, J. Thies, M. Röhrig-Zöllner, A. Bleh, J. Backhaus, A. Basermann, Simd vectorization for simultaneous solu-

- tion of locally varying linear systems with multiple right-hand sides, *The Journal of Supercomputing* 79 (13) (2023) 14684–14706.
- [19] S. Winkelmann, J. Zonker, C. Schütte, N. D. Conrad, Mathematical modeling of spatio-temporal population dynamics and application to epidemic spreading, *Mathematical Biosciences* 336 (2021) 108619. doi:<https://doi.org/10.1016/j.mbs.2021.108619>.
URL <https://www.sciencedirect.com/science/article/pii/S0025556421000614>
- [20] K. Prem, A. R. Cook, M. Jit, Projecting social contact matrices in 152 countries using contact surveys and demographic data, *PLoS computational biology* 13 (9) (2017) e1005697. doi:[10.1371/journal.pcbi.1005697](https://doi.org/10.1371/journal.pcbi.1005697).
- [21] S. Merkt, S. Ali, E. K. Gudina, W. Adissu, A. Gize, M. Muenchhoff, A. Graf, S. Krebs, K. Elsbernd, R. Kisch, et al., Long-term monitoring of SARS-CoV-2 seroprevalence and variants in Ethiopia provides prediction for immunity and cross-immunity, *Nature Communications* 15 (1) (2024) 3463.
- [22] H. Zunker, R. Schmieding, D. Kerkmann, A. Schengen, S. Diexer, R. Mikolajczyk, M. Meyer-Hermann, M. J. Kühn, Novel travel time aware metapopulation models: A combination with multi-layer waning immunity to assess late-phase epidemic and endemic scenarios, *medRxiv* (2024). doi:[10.1101/2024.03.01.24303602](https://doi.org/10.1101/2024.03.01.24303602).
URL <https://www.medrxiv.org/content/early/2024/03/02/2024.03.01.24303602>
- [23] T. C. Schelling, Dynamic models of segregation, *The Journal of Mathematical Sociology* 1 (2) (1971) 143–186. doi:[10.1080/0022250X.1971.9989794](https://doi.org/10.1080/0022250X.1971.9989794).
- [24] E. Hunter, B. Mac Namee, J. D. Kelleher, A Taxonomy for Agent-Based Models in Human Infectious Disease Epidemiology, *Journal of Artificial Societies and Social Simulation* 20 (3) (2017) 2. doi:[10.18564/jasss.3414](https://doi.org/10.18564/jasss.3414).
URL <http://jasss.soc.surrey.ac.uk/20/3/2.html>

- [25] R. A. Bradhurst, S. E. Roche, I. J. East, P. Kwan, M. G. Garner, A hybrid modeling approach to simulating foot-and-mouth disease outbreaks in Australian livestock, *Frontiers in Environmental Science* 3 (Mar. 2015). doi:10.3389/fenvs.2015.00017.
URL http://www.frontiersin.org/Environmental_Informatics/10.3389/fenvs.2015.00017/abstract
- [26] S. Kasereka, N. Kasoro, A. P. Chokki, A hybrid model for modeling the spread of epidemics: Theory and simulation, in: 2014 4th International Symposium ISKO-Maghreb: Concepts and Tools for knowledge Management (ISKO-Maghreb), IEEE, Algiers, Algeria, 2014, pp. 1–7. doi:10.1109/ISKO-Maghreb.2014.7033457.
URL <http://ieeexplore.ieee.org/document/7033457/>
- [27] T. Yoneyama, S. Das, M. Krishnamoorthy, A Hybrid Model for Disease Spread and an Application to the SARS Pandemic, *Journal of Artificial Societies and Social Simulation* 15 (1) (2012) 5. doi:10.18564/jasss.1782.
URL <http://jasss.soc.surrey.ac.uk/15/1/5.html>
- [28] G. V. Bobashev, D. M. Goedecke, Feng Yu, J. M. Epstein, A Hybrid Epidemic Model: Combining The Advantages Of Agent-Based And Equation-Based Approaches, in: 2007 Winter Simulation Conference, IEEE, Washington, DC, USA, 2007, pp. 1532–1537. doi:10.1109/WSC.2007.4419767.
URL <http://ieeexplore.ieee.org/document/4419767/>
- [29] E. Hunter, B. Mac Namee, J. Kelleher, A Hybrid Agent-Based and Equation Based Model for the Spread of Infectious Diseases, *Journal of Artificial Societies and Social Simulation* 23 (4) (2020) 14. doi:10.18564/jasss.4421.
URL <http://jasss.soc.surrey.ac.uk/23/4/14.html>
- [30] G. Schaller, M. Meyer-Hermann, Continuum versus discrete model: a comparison for multicellular tumour spheroids, *Philosophical Transactions of the Royal Society A: Mathematical, Physical and Engineering Sciences* 364 (1843) (2006) 1443–1464. doi:10.1098/rsta.2006.1780.
URL <https://royalsocietypublishing.org/doi/10.1098/rsta.2006.1780>

- [31] N. M. Shnerb, Y. Louzoun, E. Bettelheim, S. Solomon, The importance of being discrete: Life always wins on the surface, *Proceedings of the National Academy of Sciences* 97 (19) (2000) 10322–10324. doi:10.1073/pnas.180263697.
URL <https://pnas.org/doi/full/10.1073/pnas.180263697>
- [32] J.-H. Niemann, S. Uram, S. Wolf, N. Djurdjevac Conrad, M. Weiser, Multilevel optimization for policy design with agent-based epidemic models, *Journal of Computational Science* 77 (2024) 102242. doi:<https://doi.org/10.1016/j.jocs.2024.102242>.
URL <https://www.sciencedirect.com/science/article/pii/S1877750324000358>
- [33] S. Winkelmann, C. Schütte, The spatiotemporal master equation: Approximation of reaction-diffusion dynamics via Markov state modeling, *The Journal of Chemical Physics* 145 (21) (2016) 214107. doi:10.1063/1.4971163.
URL <http://aip.scitation.org/doi/10.1063/1.4971163>
- [34] D. T. Gillespie, Exact stochastic simulation of coupled chemical reactions, *The Journal of Physical Chemistry* 81 (25) (1977) 2340–2361, publisher: American Chemical Society. doi:10.1021/j100540a008.
URL <https://doi.org/10.1021/j100540a008>
- [35] M. J. Kühn, D. Abele, D. Kerkmann, S. A. Korf, H. Zunker, A. C. Wendler, J. Bicker, D. K. Nguyen, R. Schmieding, L. Plötzke, et al., MEMilio - a high performance Modular EpideMIcs simuLatIOOn software (2023). doi:10.5281/zenodo.10412635.
URL <https://doi.org/10.5281/zenodo.10412635>
- [36] N. Djurdjevac Conrad, L. Helfmann, J. Zonker, S. Winkelmann, C. Schütte, Human mobility and innovation spreading in ancient times: a stochastic agent-based simulation approach, *EPJ Data Science* 7 (1) (2018) 24. doi:10.1140/epjds/s13688-018-0153-9.
URL <https://epjdatascience.springeropen.com/articles/10.1140/epjds/s13688-018-0153-9>
- [37] C. L. Vestergaard, M. Génois, Temporal Gillespie Algorithm: Fast Simulation of Contagion Processes on Time-Varying Networks, *PLOS Computational Biology* 11 (10) (2015) e1004579. doi:10.1371/journal.

pcbi.1004579.

URL <https://dx.plos.org/10.1371/journal.pcbi.1004579>

- [38] M. Schmidtchen, O. T. C. Tse, S. Wackerle, A multiscale approach for spatially inhomogeneous disease dynamics, *Communication in Biomathematical Sciences* 1 (2) (2018) 62–87, number: 2. doi:10.5614/cbms.2018.1.2.1.

URL <https://journals.itb.ac.id/index.php/cbms/article/view/5768>